Review Article **Open Access**

Zhizhen Ma, Zhuoran Li, Ke Liu, Chenran Ye, and Volker J. Sorger*

Indium-Tin-Oxide for High-performance Electro-optic Modulation

DOI 10.1515/nanoph-2015-0006
Received September 29, 2014; accepted March 24, 2015

Abstract: Advances in opto-electronics are often led by discovery and development of materials featuring unique properties. Recently, the material class of transparent conductive oxides (TCO) has attracted attention for active photonic devices on-chip. In particular, indium tin oxide (ITO) is found to have refractive index changes on the order of unity. This property makes it possible to achieve electro-optic modulation of sub-wavelength device scales, when thin ITO films are interfaced with optical light confinement techniques such as found in plasmonics; optical modes are compressed to nanometer scale to create strong light-matter interactions. Here we review efforts towards utilizing this novel material for high performance and ultra-compact modulation. While high performance metrics are achieved experimentally, there are open questions pertaining to the permittivity modulation mechanism of ITO. Finally, we review a variety of optical and electrical properties of ITO for different processing conditions, and show that ITO-based plasmonic electro-optic modulators have the potential to significantly outperform diffraction-limited devices.

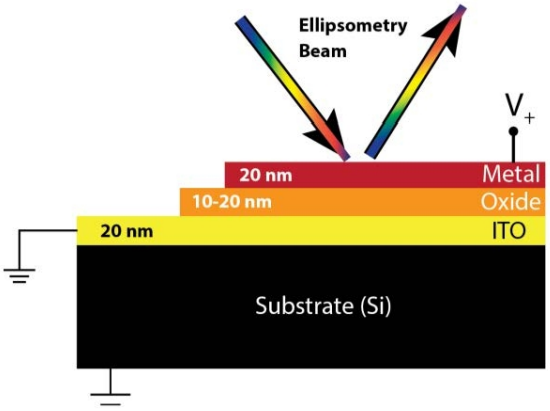

The unique electro-optic properties of indium tin oxide (ITO) such as unity refractive index modulation and epsilon-near-zero (ENZ) behavior allow for new functionality of active photonic devices on-chip. However, processing conditions and physical non-concurrencies in recent work have led to question in the field. Here we review recent advanced of ITO processing and devices specifically for electro-optic modulation; we highlight promising results and point to open research directions.

1 Introduction

A potential viable way of fulfilling both size and power requirement for future photonic integrated circuit (PIC) technology lies in down-scaling opto-electronic devices beyond the diffraction limit of light [1–4]. The advantage of such sub-diffraction limited photonics is two-fold; reduced optical power requirements and physical device size. To elaborate on this, while being physically compact, the optical mode confinement of such components can strongly enhance light matter interactions (LMI) [5, 6], which can reduce required drive power to obtain the desired effect, for example, signal modulation, optical non-linearities [7, 8]. In order to address these demands, photonic components and even circuits based on surface plasmon polaritons (SPPs), collective oscillations of electrons at metal-dielectric interfaces are thought of a solution for nanoscale PICs [9]. However, while SPP-based schemes have been explored before, many do not offer both sub-wavelength confinement beyond the diffraction limit and long enough interaction lengths making these designs often unsuitable towards nanoscale photonic integration [10, 11]. As a result, the use of plasmonics for photonic on-chip solutions, in particular for optical interconnects remained uncertain until recently. However, emerg-

***Corresponding Author: Volker J. Sorger:** Department of Electrical and Computer Engineering, School of Engineering and Applied Science, George Washington University, Washington, DC 20052, USA; Email: sorger@gwu.edu.
Zhizhen Ma, Zhuoran Li, Chenran Ye: Department of Electrical and Computer Engineering, School of Engineering and Applied Science, George Washington University, Washington, DC 20052, USA
Ke Liu: Department of Electrical and Computer Engineering, School of Engineering and Applied Science, George Washington University, Washington, DC 20052, USA; The Key Laboratory of Optoelectronics Technology, Ministry of Education, Beijing University of Technology, Beijing 100124, P.R. China

ing materials such as the recently explored transparent conductive oxides (TCOs) show promise to deliver greatly enhanced functionality and performance.

One possible path for future photonic technology is to decouple passive light routing from active light-manipulation leading to hybrid integration strategies [8]. To this end, a low-loss platform would build the backend data link, for example, silicon-on-insulator (SOI) based waveguides [12], while SPP-based components offer compact and efficient light manipulation [5, 6, 13–16]. Therefore, these components are required to fulfil two design criteria; strong mode confinement and a sufficiently long propagation length to utilize the mode towards light manipulating effect or signal [17, 18]. Both criteria combined can be used to form a figure-of-merit (FOM) suitable for comparing design concepts towards highly scaled integrated nanophotonic building blocks as will be discussed below. A remaining challenge, however, is then given by the need to reduce the optical coupling loss arising from the optical mode size mismatch between the diffraction limited and sub-diffraction limited modes in the passive and active regions of the PIC, respectively [19]. In addition to the LMI enhancements, the choice of the optical active material is critical; towards enhancing the device performance for on-chip photonic building blocks, a variety of novel materials are emerging in recent years. These materials inhibit unique properties for nanoscale optoelectronics such as high carrier density for a tuneable permittivity. Here, we discuss a particular material indium-tin-oxide (ITO), which belongs to the family class of TCOs. By reviewing material fundamentals and recent work in nanophotonics, we show that using ITO and nanophotonic field enhancement techniques produce the aforementioned high FOM devices as exemplified by the first λ-scale electro-optic modulators (EOM) [20].

2 Transparent Conductive Oxides Used in Photonics

TCOs are widely used for their optically transparent yet electrically conductive properties. As such, TCO's found increasing interest in optoelectronic technologies such as for displays (i.e. flat panel displays) and energy conversion (i.e. photovoltaics, architectural and window glass). The discovery of TCOs dates back about one century, where Badeker found the resistivity of CdO to be as low as 1.2×10^{-3} Ω·cm. Note, this is about one order of magnitude higher than that of ITO films – the widely used TCO material today [21]. Tin dioxide (SnO_2) made technological progress when scientists applied it as a transparent heating layer in the airplane cockpit windows [22]. The broad industrial utilization of TCO materials occurred at the end of the 1960s, when infrared light filters composed of Tin or In_2O_3 were used on low-pressure sodium discharge lamps for increasing the lamp efficiency by reducing heat losses [23, 24]. Afterward,with the advent of flat-panel display technology around 1970, ITO became the most commonly used TCO material for transparent electrodes [25]. Until now, ITO is the TCO material having with the lowest resistivity (i.e. order of $1–2 \times 10^{-4}$ Ω·cm), which is widely utilized as the transparent electrodes in flat-panel displays [28, 29].

Table 1 summarizes the most promising mechanisms of modulation and its corresponding materials. In 2010, the Atwater group found the characteristic of unity order refractive index change for TCO materials, and gave ways to utilize TCO films as an active material in EOM, which could lead to a new generation of fast, on-chip, nanoscale devices with unique capabilities. The mechanism for TCO films as an active material in EOMs resembles the electrostatics found in metal-oxide-semiconductor (MOS) capacitors, a bias voltage can change the carrier concentration in an accumulation (or inversion) layer of a modulator device. This carrier change has been found to result in a refractive index change, therefore an intensity modulation could be achieved. This modulation mechanism of carrier concentration has been deployed in semiconductor modulators for many years. As an example, carrier-effect based silicon optical modulators (e.g. carrier-depletion) may reach a modulation speed of over 50 Gbps [30]. However, these devices still suffer a weak LMI (i.e. refractive index change of 2×10^{-3} at a wavelength of 1.55 μm with 10^{18} carriers/cm^3 [31]) and then a larger device footprint. The behavior of phase transition (i.e. a semiconductor to metal phase transition) is observed in some smart materials, presenting a noticeable permittivity change between the two phases. For example, vanadium dioxide (VO_2) has been studied extensively in the last decade because of its large, reversible change in its electrical, optical, and magnetic properties at a temperature close to room temperature. At room temperature VO_2 behaves as a semiconductor with a band gap of ~1 eV. At temperatures higher than 68°C VO_2 passes through an abrupt transition to a metallic state. This process is reversible when lowering the temperature below 65°C (VO_2 becomes semiconductor again). Taking advantage of the phenomenon, a compact VO_2-based absorption modulator at 1550 nm wavelength on a SOI platform can be realized through the stimuli of substrate heating [32]. The thermo-optic effect results from a temperature dependent refractive index of a material,

Table 1: Comparisons of a variety of active EO materials [36]. TCO's allow for strong optical modulation due to their ability to modulate the carrier density over several orders of magnitude electrically. However, typically, optical losses are high.

Mechanism	Active material	Advantage	Challenge
Carrier concentration change	Si	Fast, low loss	Weak response
	III-V		
	Graphene		
	TCO (ITO, GZO, AZO)	Fast, significant response	Lossy
Phase transition	VO_2, Ga, $BiFeO_3$, $BaTiO_3$, etc.	Significant response	High energy per bit Low-speed ($1\mu s$)
Thermo	Polymers		

such as in tuning the refractive index of silicon via resistive heating (i.e. ~1.8×10^{-4}/K of thermo-optic coefficient of Silicon) [33]. Another widely used thermo-optic effect material is polymer, which has the advantages of low density and refractive index, less dispersion, cheap manufacturing cost, easy to make complex shapes, and good electrical insulation. However, these types of materials suffer shortcomings such as limited temperature usability, degraded time dependence of properties (e.g. electro-optic polymers), and fatigue and solvent sensitivity. Although polymer-based thermo-optic modulators (and switches) have several drawbacks such as significant power consumption, slow transition time (usually > 1 μs), the mechanism shows operational devices and sub-systems on-chip [34, 35]. Phase transition and thermal-optic effect based modulators can provide significant response, however the time frame is high and allows for an operation speed on the order of MHz [36].

TCOs such as ITO, GZO (ZnO: Al), and AZO (ZnO: Ga) have very similar properties and allow for an efficient change of carrier concentration. As an outstanding representative of TCO materials used for EOMs, ITO exhibits its unique advantages, such as epsilon-near-zero (ENZ) in the near infrared regime and electrically tunable permittivity [37, 38]. A recently explored example of MOS-based EOM is an ITO-SiO_2-Au stack in a SOI waveguide [20]. The effective index of ITO changes from being a dielectric to a quasi-metallic state when a voltage bias is applied. Such a modulator exhibits a low insertion loss of ~1 dB for the 5 μm long device, a sub-wavelength compact size of 0.78 λ, and the broadband operation of > 500 nm with a non-resonant MOS mode [39]. Though TCO materials have a strong electro-optical response compared to the aforementioned materials (Table 1). A large index change (real part) is also accompanied by a significant extinction coefficient change (imaginary part of index) making TCOs often rather lossy due to the Kramers–Kronig relations. However, since the carrier concentration of TCOs may be selectively controlled in a post-processing, local resistivity tuning step. This allows separating the optically active material from the passive electronic, and may be realized by a plasma treatment process to optimize the resistivity of TCO layer as discussed in detail below. In the remaining sections, we specifically focus on material, processing and electro-optic modulation details for the material ITO.

3 ITO Material Science and Processing Fundamentals

ITO sputtering targets typically consist of 10% SnO_2 to 90% In_2O_3 by weight. ITO has been widely adopted by the solar industry as a transparent electrode due to both its high optical transmittance yet high electrical conductivity. In addition to the photovoltaic applications, new possibilities for ITO are emerging for electro-optic modulation. However, ITO has been found to be a difficult material to work with due to its processing invariances. In this review, we first focus on ITO's fundamental properties, and in a second step relate them to the device details of high-performance EOM.

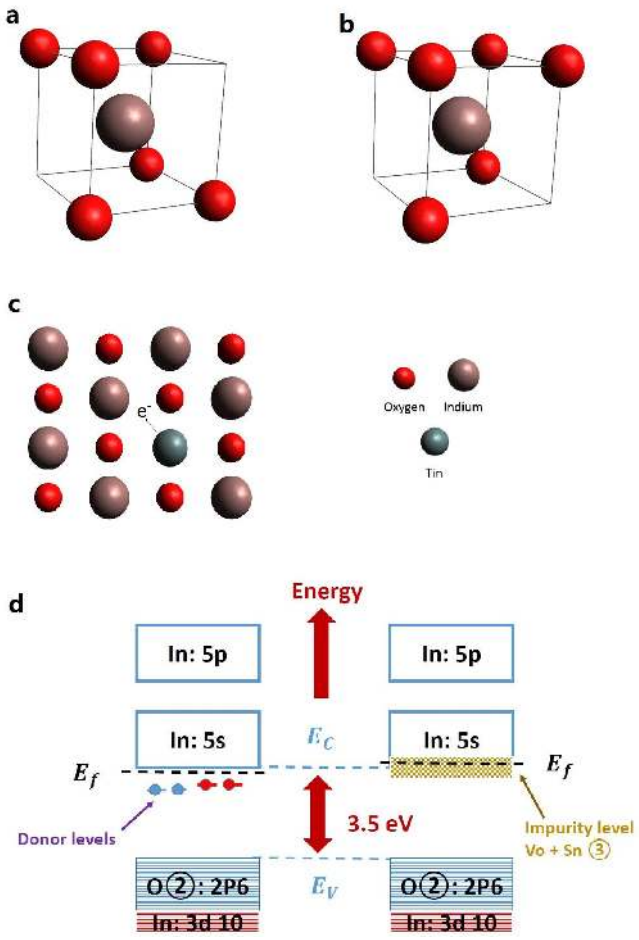

Figure 1: Indium oxide structure. (a) Eight oxygen atoms are situated within a compressed octahedra (b site) and have six equidistant oxygen atom neighbors at 2.18 Å. (b), Eight indium atoms are situated at the corners of a highly distorted octahedron (d site). For these indium atoms, there are three possible cation-oxygen distances: 2.13, 2.19 and 2.23 Å [42]. (c), Sn doping sites in an In_2O_3 lattice [48]. (d) Schematic energy-band model for tin doped indium oxide, where E_f, E_y and E_c is the Fermi energy, the violation band energy and the conduction band energy respectively. Left: low doping level, right: high doping level [45].

3.1 Indium Oxide and Tin doped Indium Oxide Structure

The atomistic structure of a unit-cell of ITO resembles that of indium oxide (In_2O_3), with the latter being an ionically bound semiconducting oxide, which crystallizes in a cubic bixbyite-type structure with a space group Ia3 and a lattice constant of 10.118 nm [40]. The unit cell of ITO contains 80 atoms, and the indium cations are located in two different six-fold-coordinated sites. One-fourth of the cations are located in trigonally compressed octahedral, referred as *b* sites (In-O distance: 2.18 Å), while the remaining three-quarters are located on highly distorted octahedral *d* sites (set of three In-O distances: 2.13, 2.19 and 2.23 Å) [41]. As Fig. 1a& 1b, indium atoms, on both *b* and *d* sites, reside at the center of a distorted cube with the six corners occupied by oxygen atoms, while the remaining two corners are empty. In the case of the *b* sites, oxygen vacancies are located along the body diagonal; for the *d* site they are located along a face diagonal [41, 42]. Figure 1c shows tin (Sn) doping sites in an indium oxide lattice, where the Sn atom occupies an interstitial site and contributes an electron (i.e., a donor), making the doped indium oxide into indium tin oxide.

3.2 Indium Oxide and ITO Band Structure

The actual material properties of ITO have been found to be highly sensitive to the processing conditions [43]. While the detailed insights of band structure, as a function of processing parameters is desirable, the band structure is a function of the complex unit cell lattice and respective electronic interactions. Therefore, the properties are usually discussed in terms of an assumed band diagram consisting of an isotropic parabolic conduction band [41, 44]. A first attempt for its description was made by Fan and Goodenough [45] who proposed the schematic energy band model for indium oxide and ITO, which allows for a qualitative explanation of the observed high optical transparency and electrical conductivity in ITO (Fig. 1d). In Fan's band model, indium oxide exhibits a wide direct band gap (3.5 eV) prohibiting interband transitions in the visible range and hence making it transparent within this frequency range, which is still the reference model used today for ITO. The conduction band was proposed to arise mainly from the indium 5s orbitals and the valence band from oxygen 2p electrons. The Fermi energy E_f is found a few eV's below the conduction band due to n-type doping of the Tin impurities [41]. The bands are slightly different; for low doping density donor states are formed just below the conduction band, and the Fermi energy lies between the donor level and the conduction band minimum (Fig. 1d). However, for very high doping, the donor density increases. Note that the donor states merge with the conduction band at a certain "critical" density, n_c, known as the Mott density defined by $\frac{n_c^{1/3}}{a_0^*} = 0.25$ for ITO, where the effective Bohr radius $a_0^\star$ is about 1.3 nm for In_2O_3 resulting in $n_c(\text{ITO}) = 3.43 \times 10^{-19}$ cm^{-3} [41]. Above the critical Mott density, the impurities and the associated electrons occupy the bottom of the conduction band forming a degenerate electron gas, and the electron gas in-

creases the ionized-impurity scattering and reduces the mobility [46, 47].

3.3 Optical and Electrical Properties of ITO

In order to utilize ITO for nanophotonic devices, a detailed knowledge and parameter interdependencies relating to the optical and electrical properties must be known. In general, the optical properties were previously modeled by a Drude–Lorentz model, due to the high carrier concentration as we discuss further below [49]. Focusing here on the electrical properties, the carrier concentration and mobility of ITO have been found to vary widely with process conditions for the deposition method such as sputtering power, oxygen flow, and annealing temperature. We therefore limit the discussion to a few key observations based on ITO's resistivity ($\rho = \frac{1}{ne\mu}$, where n is the carrier concentration, μ is the mobility and e is the free electron charge). For ITO, electrons are the majority carriers originating mainly from the doping donor Sn and oxygen vacancies. Therefore the carrier concentration of ITO films depends on the oxygen vacancy concentration, and the Sn doping levels. The latter is important since substituting an indium atom frees an electron increasing the carrier density. However, doubly-charged oxygen vacancies and singly-charged Sn on an indium site reduce the mobility of charge carriers due to ionized-impurity scattering [41]. Based on this understanding of ITO's doping interplay, the resistivity for ITO films can be tuned, either to a minimum such as for photovoltaic applications, or to a high-resistivity level. The latter is significant for electro-optic modulation as is discussed in section 4 in more detail.

Matrion *et al.* provided a useful, yet qualitative, overview linking the apparent as-deposited color of ITO films to the films resistivity, and the O_2/Sn doping concentration (Fig. 2a) [48]. The observed resistivity minimum (i.e. 'well') depending on both the O_2 and Sn doping levels, does explain the empirically observed challenge to tune ITO's resistivity; that is, the resistivity is high for low doping concentrations due to low carrier concentration, and low for high doping due to scattering from oxygen vacancies which reduce the mobility. Moreover, the observed apparent film illustrates that the higher doping could induce a particular state "extinguishing" Sn, but the high oxygen flow could not be well related to the color on the right side [41].

Interestingly, another group found the other resistivity-well trend as a function of sputtering power density (Fig. 2b) [50]. Increasing the power density creates ionized impurity centers, which induce scattering of the free electron carriers and then reduce the mobility. The gradual increase in the carrier concentration between a power density of 1 and 3 W/cm^2 is closely associated with the increased number of substituted Sn ions in the lattice. Increasing the sputtering power density further results in a flat carrier concentration due to a cancellation effect, which is from the increased level of Sn ion substitution and the decreased number of oxygen vacancies from the increased ITO film crystallinity. Many groups reported strong resistivity decreases with higher annealing temperatures; note that the annealing temperature leads to the related physical behavior as for the power density, as shown by the similar curve trends (compare Fig. 2b& 2c). However, the outlier data point (i.e. last data point for carrier concentration in Fig. 2c) actually drops instead of keeping constant, which may possibly be caused by the different oxygen flows used. Lastly, tuning with the oxygen flow the resistivity-well effect is present as well (Fig. 2d). Higher carrier densities are expected with comparatively low oxygen content and vice versa, and high mobility with increasing oxygen content, because of the enhanced crystallization. Since both mechanisms cause the opposite effects, the specific resistivity shows a minimum in the oxygen flow level. In summary, these results show explainable trends for the resistivity, and color of ITO films as a function of doping, oxygen flow, deposition power, and substrate temperature. However, it seems the error bars are still rather large, while the more quantitative data and processing details are needed towards guaranteeing a to-spec engineered ITO film electrical property.

3.4 Typical Deposition Methods

This section highlights a variety of typically deployed methods for the deposition of ITO films. The different deposition conditions for each method significantly change the optical and electrical properties of ITO film.

3.4.1 Sputtering

Sputtering is one of the most widely used techniques for the deposition of TCO films. Within sputtering, a variety of techniques have been adopted, including conventional direct current (DC), radio frequency (RF), and magnetron reactive sputtering of a metal alloy target in the presence of oxygen, as well as RF and ion beam sputtering of a pressed oxide powder target [41]. Among these options, DC and RF magnetron sputtering are the most attractive techniques

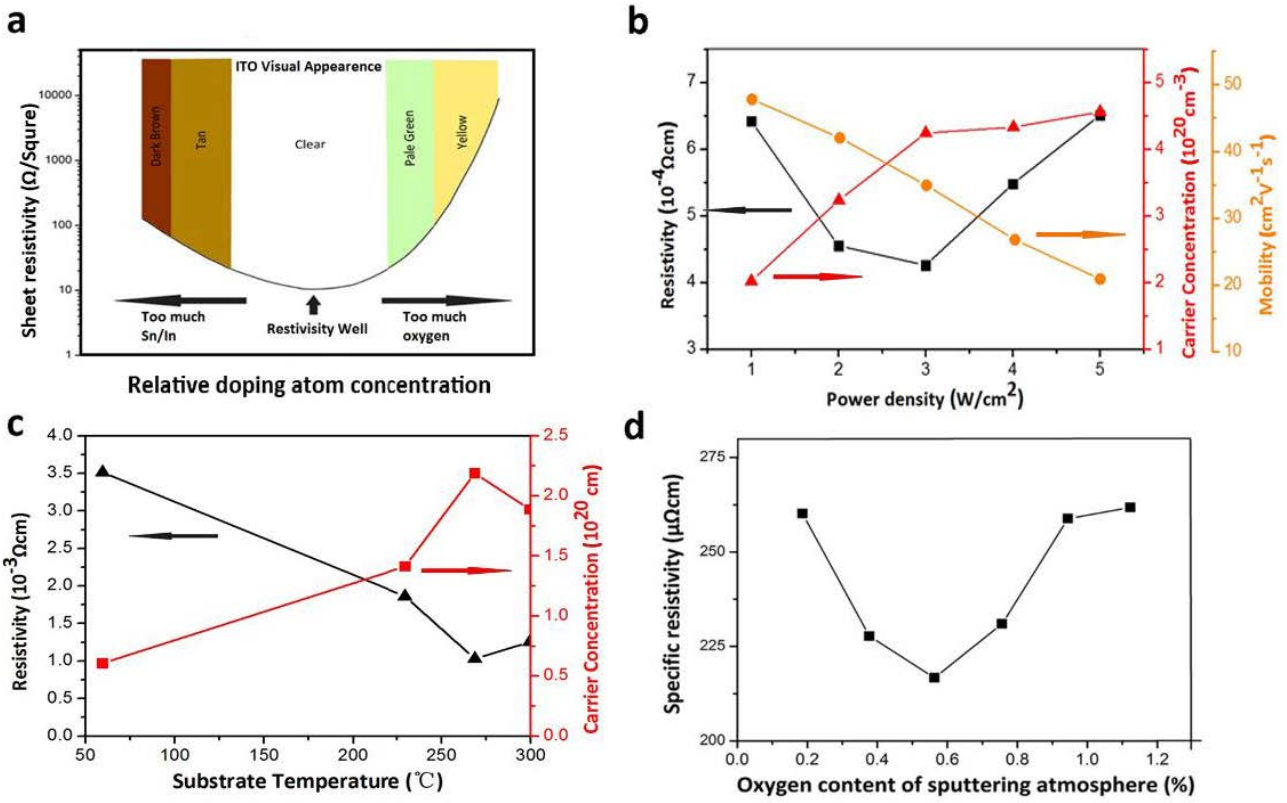

Figure 2: ITO electrical properties (a) Resistivity well effect and the color change due to different doping and oxygen concentration [48]. (b) Mobility, concentration and resistivity as a function of deposition power density [50]. (c) Concentration and resistivity with increasing substrate temperature [51]. (d) Resistivity change due to tuning oxygen flow [52].

for industrial development because both allow for high deposition rates, good reproducibility, and the possibility of using commercially available large area sputtering systems [53]. Typically, magnetron sputtering processes are performed at high substrate temperatures (≥ 200°C), as these allow the best results in terms of layer transparency and conductivity to be obtained. However, several applications, for example, solar cells and devices on plastics, require a low deposition temperature, as higher temperatures would damage the underlying either electronic device structures or substrate itself. This challenging task has been investigated by several workers where the RF technique was mostly adopted [54, 55]. The main difficulty of RF deposition at room temperature is due to insufficient recrystallization of ITO at low temperatures leading to the poor structural and electrical properties [56]. Furthermore, DC magnetron sputtering at room temperature is also challenging since the formed ITO layers are usually amorphous with a high electrical resistivity [57]. High temperature ITO sputtering can be done in DC and RF discharge plasma modes which allow layers with obtainable similar transparency/conductivity properties. Depending on the plasma mode (DC or RF), an essential difference of optimum sputtering conditions (i.e. discharge power density, pressure, oxygen concentration, etc.) was observed, as well as a difference in the crystalline structure and morphology of the formed layers [53]. In general, sputtering allows for a relatively wide range of film tunablility due to the various process conditions involved in the process. However, the very process flexibility also requires precise control of all parameters.

3.4.2 Evaporation

For evaporation methods such as electron beam evaporation and direct thermal evaporation, typical powders of metallic Sn and In are commonly used. Regarding the latter, indium will be preferentially vaporized, causing a change in the composition of the tin and indium liquid alloy with time due to the significantly higher vapor pressure of In relative to Sn [58]. That being the case, an electron beam can be a more reproducible method for low resistivity and high transparency films. Furthermore, low resistivity ITO films processed at low temperature have been reported using reactive electron beam evaporation onto

heated glass substrates (300°C and an oxygen pressure above 0.5 mT) [59]. Under optimum conditions, the resistivity is 3×10^{-4} Ω·cm with an average mean transmittance of about 84% in the visible range [41].

3.4.3 Chemical Vapor Deposition

Chemical vapor deposition (CVD) is a process in which a chemical reaction involving gaseous reacting species takes place on, or in the vicinity of, a heated substrate surface. This technique has the advantage of being cost-effective with respect to the apparatus, and enables the production of coatings with good properties without the use of high vacuum even on substrates with complicated shapes. The deposition of ITO films by the CVD method generally faces difficulties due to a lack of volatile and thermally stable source materials [41]. Under certain conditions, an ITO film with a resistivity as low as 2.9×10^{-4} Ω·cm is obtained at a reaction temperature of 400°C [41]; however, more research is needed in this field.

4 ITO for Electro-optic Modulation

ITO has recently sparked the interest for active photonic components on-chip. In particular, the research by the Atwater, Leuthold, and Sorger group had raised the interest for electro-optic (EO) modulation utilizing ITO as an active switching material [60, 61]. For instance, Sorger *et al.* demonstrated a 3-λ compact EO modulator using ITO inside a plasmonic hybrid mode [20]. In this section, we summarize these effects along with some original content on ITO processing for high-efficient EO modulation. Furthermore, we review biasing options for ITO to produce ENZ characteristics for EO modulation, and close this section by critically reviewing some outstanding questions in the field of ITO for EO modulation that shall guide the future research.

4.1 Drude Model and Refractive Index Ellipsometry

The aim for strong EO modulation is to alter the effective modal index of an optical mode traveling inside the device. Note, in this discussion we exclude localized modulation effects, that is, non-propagating modes towards maximizing the index change of the active material, Δn_{active}, while minimizing the utilized voltage bias. Since the latter is related to the electrostatics inside the EOM, this discussion is postponed to the section 5, where a variety of experimental demonstrations of ITO for next generation EO modulation are highlighted and discussed. In what follows now, we discuss the possible strength of ITO-based EO modulation, which connects ITO's index to the carrier concentration via a Drude–Lorentz model. This model has been previously used for TCOs such as ITO [62, 63], and allows us to write the complex permittivity as

$$\varepsilon(\omega) = \varepsilon_\infty - \frac{\omega_p^2}{\omega(\omega + i\gamma)};\ \omega_p^2 = \frac{n_c e^2}{\varepsilon_0 m^\star} \tag{1}$$

where γ is the electron scattering rate, ω is the angular momentum in rad/s, ε_0 and $\varepsilon_\infty = 1 + \chi = 3.9$ [35] are the free space and long-angular-momentum-limit permittivities, respectively, ω_p is the plasma frequency, $m^\star$ is the reduced mass of ITO equating to $0.35m_0$, with m_0 being the rest mass of the electron, n_c is the voltage-modulated carrier density for the ITO film, and e is the elementary electron charge. Using Eqn. 1 and sweeping the free parameter, n_c, versus the device operating frequency, the general function for the permittivity and index are obtained (Fig. 3). The Drude–Lorentz model assumes the physical EO modulation origin to be the free carrier modulation. Thus, if the carrier concentration in a waveguide-type device design can be electrically altered, then EO modulation can be expected. However, only meaningfully strong modulation can be achieved if the ITO's index change may influence the effective mode index of the device, and not just the material films index. This therefore requires the mode field enhancement techniques such as observed in plasmonics, slot-waveguides, or optical cavities. The underlying physical mechanism is to enhance the non-linear polarization of the active material leading to a permittivity and hence index change as a function of applied voltage bias. This can be done by confining the mode into sub-diffraction limited fields, which increases the field strength at the active material, and thus leads to higher modulation efficiency (i.e. extinction-ratio/V_b). It is remarkable to notice that if the carrier concentration of ITO can be changed from ~10^{19} to ~10^{21} cm^{-3}, the index changes dramatically; the real part by unity, and the extinction coefficient by about 2-orders of magnitude (Fig. 3). Since the electrostatics of a device limits the achievable change of the carrier concentration, Δn_{ITO}, it is imperative to process ITO in such a way that the as-deposited film pertains to carrier concentration as low as possible. This is important, because a given finite voltage bias will increases the carrier density by only a finite amount dictated by the electrostatics in an accumulation layer formed in an MOS capacitor. For instance the experimental results of Ref. [20] indicate an about 70 times

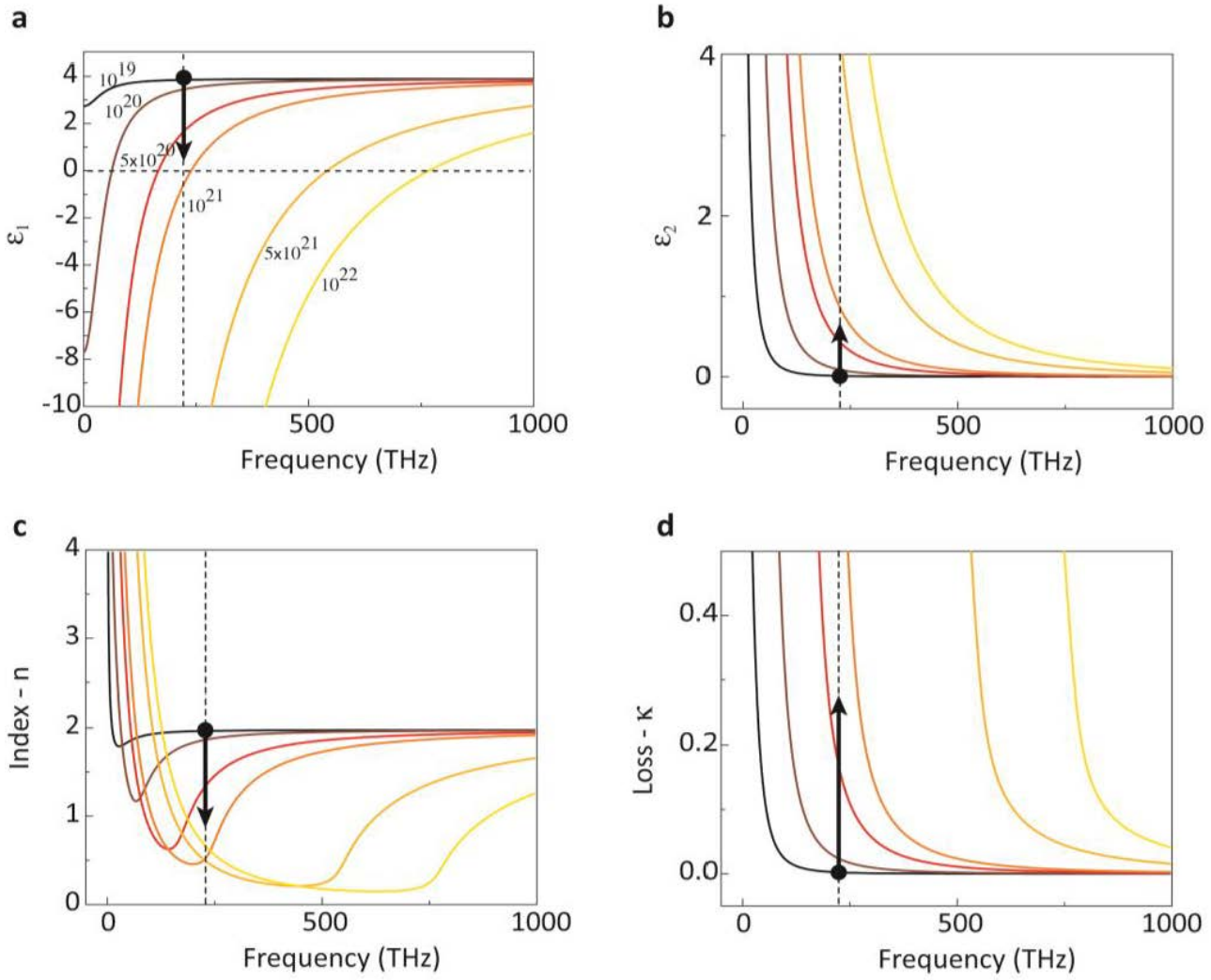

Figure 3: ITO optical film parameters. (a)&(b) ITO permittivity dispersion for various carrier concentrations. (c)&(d) Index dispersion of the active materials ITO based on the Drude–Lorentz model for various carrier concentrations [64]. Arrows indicate switching range for ON (arrow start) and OFF (arrow tip), respectively [65]. λ = 1310 nm vertical dashed line.

carrier density increase for ITO when being sandwiched in a plasmonic MOS design. Note, that the optimization goal of processing ITO to exhibit a high-resistivity for the as-deposited films is opposite to the material goals of the photovoltaic industry, which utilizes ITO as a transparent electrode, where the aim is to decrease resistivity. However, EOM devices face a double-sided challenge when it comes to ITO's resistivity; when high-speed modulation is desired requiring low RC-delays, the contact resistance to ITO should be minimized. Thus, the carrier density seems to be a trade-off of the device performance, thus balancing signal extinction ratio (ER) and low energy consumption (i.e. energy/bit) on one side, and modulation speed on the other. However, this dilemma can be bypassed via spatially selective ITO plasma treatments which n-dopes ITO in a selected region at the electrical contact (i.e. assumed ITO is being electrically contacted serving as the active material). The latter case is discussed in more detail below. The outstanding aim for an ITO-based EOM optimization is therefore to achieve low carrier concentrations of ITO during processing for the device region.

We performed a variety of experimental ITO processing tests for EO modulation, choosing the physical vapor deposition (PVD) method of sputtering to investigate effects of (a) O_2 concentration, (b) RF power, (c) bias effect such as DC vs. AC, and (d) the effect of a wafer substrate. Regarding the results, we report on two selected parameters affecting the ITO's refractive index most strongly: the oxygen flow and the RF bias, whose effect can be visually seen by the optical appearance of the as-deposited ITO film (Fig. 4a), and by ellipsometry refractive index data (Fig. 4c). At a wavelength of 1550 nm, an increase in the

O_2 chamber concentration clearly increase the refractive index, which correspond to a lower carrier concentration. It is consistent with the result of section 3, where a higher oxygen flow prohibits the existence of oxygen vacancies. However, altering the RF bias voltage induces a minor carrier concentration decrease. Note, that similar ITO film properties were observed between electron-beam evaporated films and sputtered films without oxygen flow, which can be explained by the lack of O_2 in both cases.

It is worthwhile to report our procedure and details of the performed ellipsometry tests. Variable angle spectroscopic ellipsometry (VASE) is a rather complex procedure and many physically non-meaningful results can be generated. For ITO the procedure is specifically challenging for several reasons due to (a) low signal-to-noise ratio owing to optical absorption, (b) strong dispersion (i.e. for broadband ellipsometry), and (c) vertical index variations since ITO grows commonly in graded microstructures. Following Ref. [66] we are able to provide the reliable ITO results following a 2-step procedure; ITO films are first fit with a Cauchy model over a smaller and typically less optical lossy wavelength range (i.e. 300–600 nm) to determine the film thickness. In a second step the Lorentz–Drude model is used to obtain the broadband index information using the film thickness as an input parameter. Depending on the film thickness and application a graded index profile for ITO can be assumed for more accurate results. This relates to a gradually changed index profile with the film thickness due to the formation of an accumulation layer in the EOM devices. However, even following this procedure blindly is not advised, but a second control mechanism is needed for accurate results. That is, both angular functions Psi & Delta are fitted by both a material and a layer-composition model returning a residual mean error (RME) value (Fig. 4b). We found that the RME values above 10 are to be discarded, with our results reported here having RME < 5. If higher accuracy is desired the fitting procedure should be repeated until an RME minimum is found. We also tested the Tauc-Lorentz model for the step-1 fit, which provided the relatively stable results. As for the data presented here, an increase in oxygen flow shifts ITO to drop its loss, in accordance to the Kramers-Kronig (KK) relations, increase its refractive index (real part). A higher sputtering RF bias voltage has a similar effect, however with less severity than oxygen.

Of particular interest for EOMs is a material's ability to change its refractive index as a function of voltage bias. Early tests by Feigenbaum *et al.* performing ellipsometry on metal-oxide-ITO-metal heterostructures left the field with open questions [60]; the group argued that a capacitive accumulation layer is formed at the ITO-SiO_2 interface

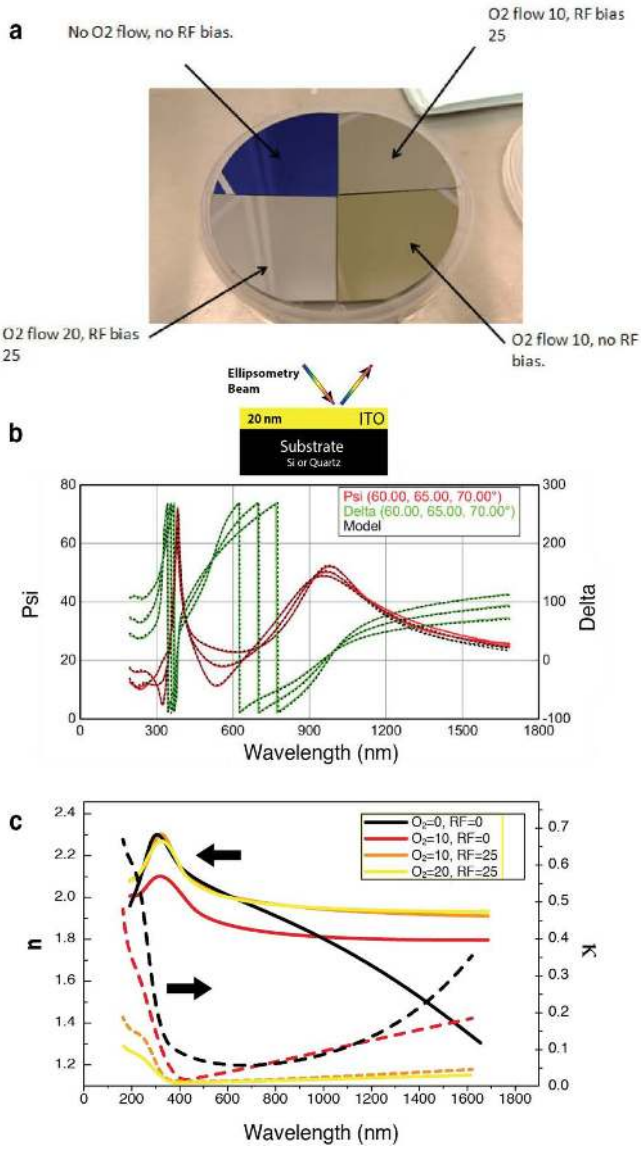

Figure 4: Optical performance measurements of ITO samples using variable angle spectroscopic ellipsometry method. (a) Photography of four ITO samples with a variety of experimental ITO processing tests (i.e. different combinations of oxygen flow and RF bias), showing different appearance of ITO films. O_2 flow in sccm, and RF bias in volts. (b) The angular functions, Psi & Delta as a function of wavelength range, where Psi is the ratio of the amplitude diminutions and Delta is the phase difference induced by the reflection, both were measured by ellipsometry method. (c) The measured results of refractive index (n is the real part and κ is the imaginary part) as a function of wavelength range with different oxygen flow and RF bias.

leading to the ITOs index modulation (Fig. 8 below). However, these data showed a decreasing loss with increasing carrier concentration, which appears non-physical or at least, unlike trends found in semiconductors. Moreover, as the loss decreases with bias, the real part was found to decrease simultaneously which seemingly violates the KK

relations. It is for these non-congruent findings, that we repeated the biased ITO VASE experiments following the above-described methodology. In addition these measurements are extended into the telecommunication frequency range. Unlike Ref. [60] we find an increase of the ITO's loss with a bias voltage, which denotes an increase in optical loss due to carrier accumulation at the ITO-oxide interface (Fig. 5). Noteworthy is the sudden index jump with voltage and range; we note an increase from about 0.006 – 0.14 for the top 5 nm of a graded ITO film. Critical point for low RME is that the top metal acting as an electrode is semi-transparent. For the top metal contact a skin-depth thickness is selected for a wavelength in the NIR.

A band diagram analysis shows the band bending of the ITO layer at the ITO-SiO_2 interface (Fig. 5c). Note, ITO conduction band drops below the Fermi level, resulting in an accumulation of electrons for positive voltage bias at the top-metal contact. Note, this is consistent with the measurements from Ref. [20], where no modulation effect was observed for a negative voltage bias. Furthermore, the electrostatic of the MOS capacitor is primarily governed by the 'gate' oxide layer (i.e. thickness and dielectric constant). Naturally, a stronger (weaker) electrostatics on the ITO layer, that is, thinner (thicker) $t_{gate-ox}$, leads to an earlier (delayed) turn-on of the optical loss and hence OFF-state of an electro-absorption modulator. On the other hand a thinner $t_{gate-ox}$ also leads to a larger EOM device capacitance slowing down the 3-dB bandwidth. It is therefore interesting to note, that $t_{gate-ox}$ is a trade-off EOM device parameter that should be optimized for a specific EOM performance (i.e. low power, or high speed).

4.2 ITO Selective Contacts

Above we argued that in order to achieve a high modulation depth (i.e. extinction ratio) for EOMs, ITO should be deposited for a low-loss state (i.e. ON-state in EOM terminology), because raising the carrier density via a voltage bias increases optical loss shifting the EOM into the absorption (OFF) state. However, if ITO is to be electrically contacted, this poses a dilemma since ITO's low-loss state comes with low carrier concentration, and hence high resistivity specifically for thin films below 50 nm thickness. The latter makes high-modulation speeds challenging due to the limited RC delay time of the high resistive contacts. A potential solution explored here is to deposit ITO in a low-loss state at the device area, but then selectively treat ITO at the contact area. Since micrometer-scale local annealing is challenging, we explored selective plasma treatment. This method exposes ITO to an O_2 plasma thus dop-

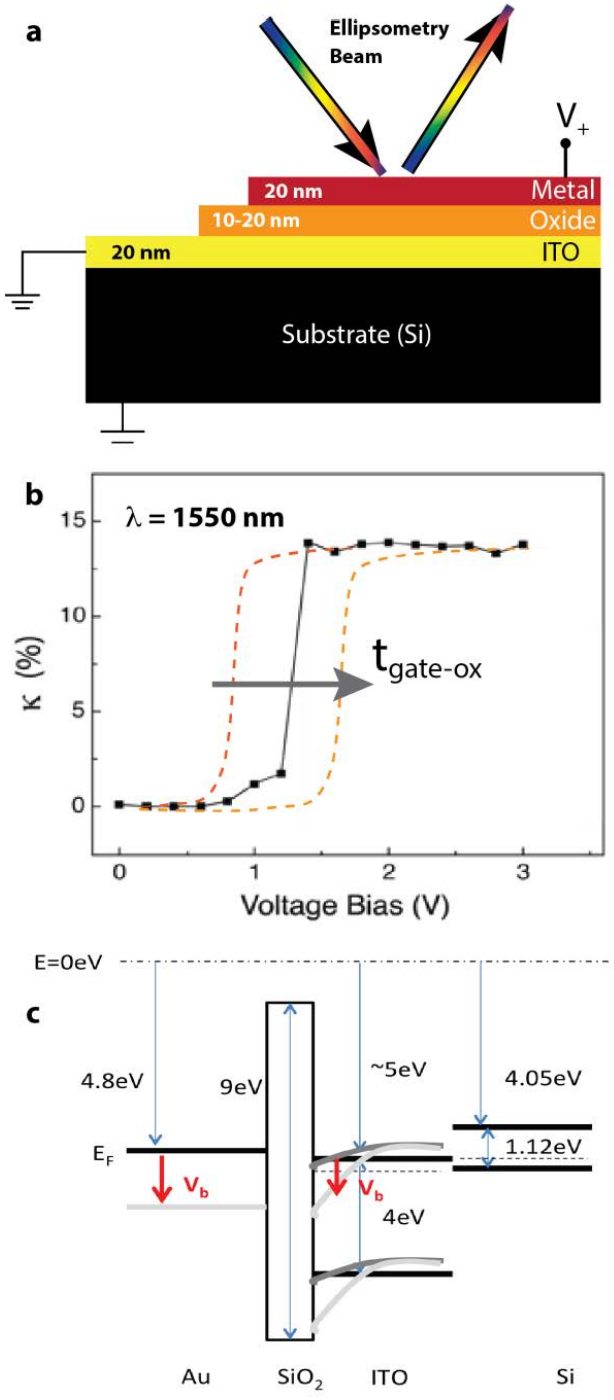

Figure 5: Dynamic VASE on ITO MOS structures to determine the optical loss change as a function of voltage bias. (a) Setup schematic. Note, no significant change in the results were recorded when ITO or the doped silicon substrate was contacted. Oxide = SiO_2 (ALD), metal = Gold. ITO and Au were sputtered. (b) ITO film extinction coefficient vs. bias voltage shows a strong modulation. Graded ITO film, results for top 5 nm. (c) Band diagram of the ITO-MOS design identifying the ITO-SiO_2 interface for the charge accumulation region.

a

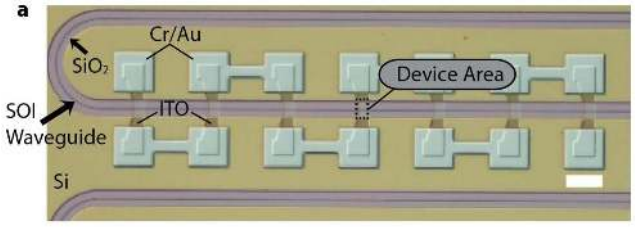

b

Sample	Si/ITO O_2=20 sccm Annealed = no Plasma = no	Si/ITO O_2=20 sccm Annealed = 300C, Plasma = no	Si/ITO O_2=20 sccm Annealed = no Plasma = Yes	Si/ITO O_2=20 sccm Annealed = 300C Plasma = Yes
Resistivity [Ω-cm]	$[10^{-2}$-10]	~10^{-3}	$[10^{-4}$-$10^{-3}]$	~10^{-4}

Figure 6: Resistivity of ITO films and contact pads. (a) Micrograph of a test structure for transmission line method (TMD) resistivity tests. Note, the ITO film covers the sidewalls of the SOI waveguide. Scale bar 50 μm. (b) Effect of the sputtering ITO films and annealing. Annealing at T = 300°C for 30 min. Plasma treatment, O_2 flow-rate ~30 sccm, exposure time = 5 min.

a

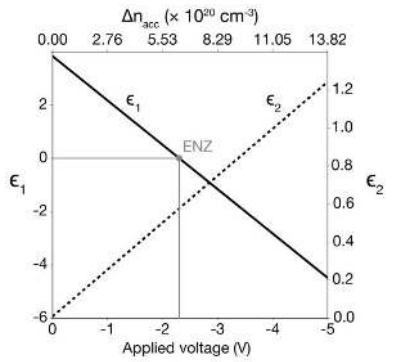

b

Device	ER, dB/μm	α_{min}, dB/μm	FoM	λ, nm	Based on	Date
SPPAM	2	24	0.08	1550	MIM	04/2011
3λ-size	1.0	0.04	25	1310	Si-wg	04/2012
Tunable ENZ	18	1	18	1310	Si-wg	06/2012
Tuned ε	3	9	0.3	1550	MIM	07/2012
wire-MIM	13	11	1.2	1550	MIM	09/2012
Sub-λ-size	6	0.7	8.5	1310	Si-wg	07/2013
Slot	2.5-11	0.85	3-13	1550	Slot-wg	10/2013
ENZ-Si	0.10	0.003	37	1550	Si-wg	11/2013
GZO-Si	24	0.06	400	1550	Mult-wg	11/2013
TiN-Si	46	0.3	160	1550	Mult-wg	11/2013

Figure 7: (a) Epsilon-near-zero (ENZ) condition for the ITO after Ref. [37]. Bringing the real part of the material close to zero can result in large modal index changes of nanostructured waveguides. (b) Comparison table of ultra-compact EOMs based on various TCO materials, where ER is the extinction ratio, α_{min} is the minimum attenuation, and FOM is the figure of merit. [36].

ing the contact. Figure 6 summarizes 4-probe resistivity results for the various process conditions. The EOM optimized deposition method yields the expected high resistivity, but annealing and more importantly an exposure to O_2 plasma reduces the resistivity by several orders of magnitude. While these results are encouraging, a more in-depth study should be carried out to map-out this effect in detail, and we invite readers to perform this study.

4.3 Epsilon Near Zero ITO for Modulation

Recently, the field of ultra-compact EO modulation has turned some attention to the concept of ENZ materials, where the real part of permittivity is electrically tuned based on the Drude model [37]. Using free carrier density tuning can lead to a regime where the real part of index approaches zero, which in turn results in a dramatic change in the optical property of the material. Figure 3a above showed the carrier concentration condition where the ENZ effect occurs in ITO, which happens around a carrier concentration of about 10^{21} cm^{-3} around a telecom frequency. It is interesting to note, that the experimental results of Ref. [20] where very close to this bias point, and hence are the first experimental evidence of this effect (even though the authors did not label it as an ENZ effect). The detailed picture is that ENZ materials impose a unique boundary condition onto electric fields (i.e. of nearby waveguides). This is a direct consequence of the continuity condition of the normal component of the electric field displacement, and leads in turn to large field enhancements inside the ENZ material relative to the adjacent layer. It is the physical property of TCOs and hence ITO that makes them attractive for EO modulation applications. Recently, a few groups have explored this ENZ effect numerically; for instance, Z.L. Lu *et al.* numerically reported an electroabsorption modulator based on tunable aluminum-doped zinc oxide (AZO) materials and slot waveguides [38]. The AZO layer employed as the active slot serves as an ENZ material, which can be tuned between ENZ (high absorption) and epsilon-far-from-zero (low absorption) by accumulation carriers. A.P. Vasudev *et al.* proposed a similar MOS-capacitor based modulator consisting of a nanowire SOI waveguide coated with layers of 5 nm HfO_2 and 10 nm ITO [37]. Babicheva *et al.* numerically and analytically explored a variety of TCO EOM designs introducing a figure of merit for absorption modulators defined as

$$FOM = \frac{|Im(k_{eff})_{on} - Im(k_{eff})_{off}|}{Im(k_{eff})_{state}} = \frac{ER}{\alpha_{min}} \qquad (2)$$

where the extinction ratio is defined by $ER = \frac{10\log\left(\frac{P_{on}}{P_{off}}\right)}{L} = 8.68\left(Im(k_{eff})_{off} - Im(k_{eff})_{on}\right)$ (Fig. 7b) [36]. Benchmarking a variety of ultra-compact EOMs with Eqn. 2 shows that theoretically very high-performance EOMs are possible. Note, that this comparison does mix the experimental demonstrations with the numerical proposals.

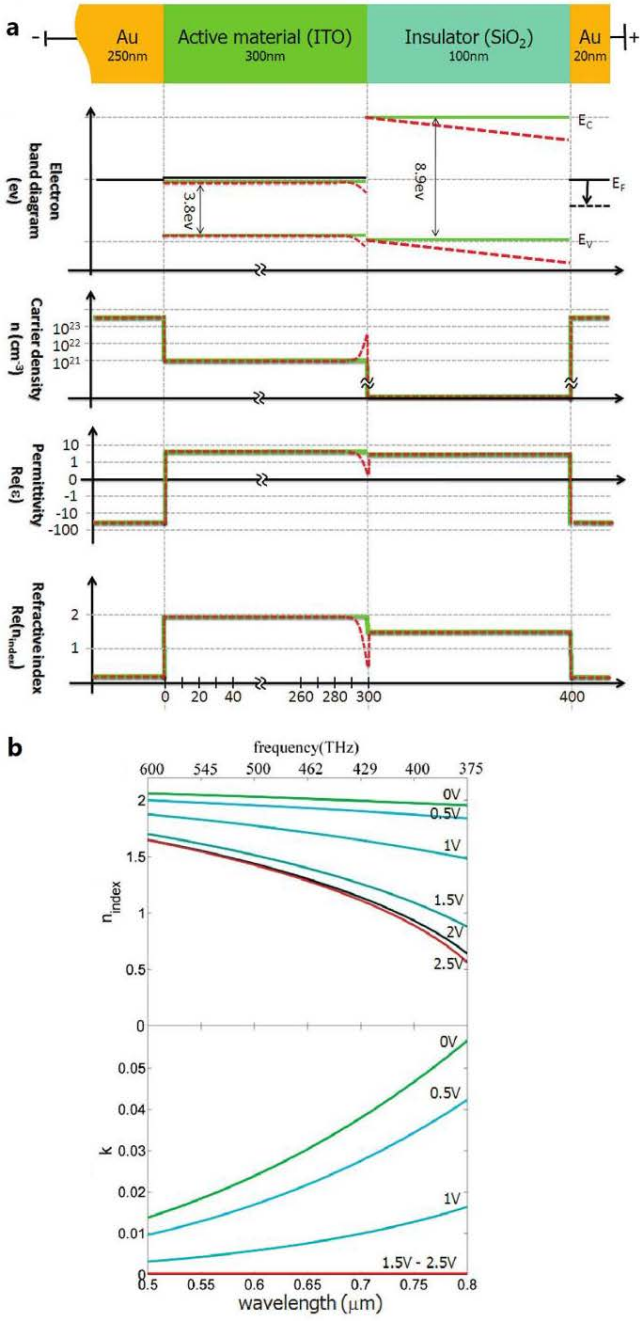

Figure 8: (a) MOS structure with (dashed red) and without (solid green) charge accumulation [60]. From top to bottom are the structure schematics, band diagram, carrier concentration, permittivity and refractive index, respectively. (b) The complex refractive index (n for the real part and κ for the imaginary part) in a 5 nm accumulation layer, extracted from the ellipsometry data.

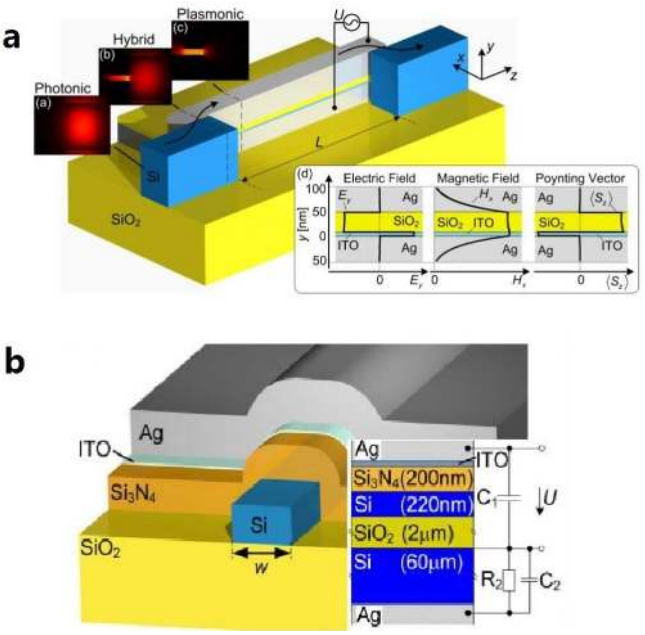

Figure 9: (a) Schematic of the waveguide-integrated, silicon-based nanophotonic modulator [61]. The MOS design features a plasmonic optical mode, which concentrates the mode's electric field and allows for a good overlap with the active ITO layer. (b) 3D schematic of the fabricated device and its lumped element model describing the low-pass characteristic of the device.

5 EOM Devices based on ITO

Based on the potential for active EO modulation using ITO discussed above, this section reviews some initial experimental work demonstrating EOMs. In 2010, the Atwater group reported a method for obtaining unity-order refractive index changes in the accumulation layer of a MOS heterostructure with ITO as the active material [60]. This pioneering work demonstrated a local Δn_{index} of 1.5 in the ITO film using plasmonic mode confinement as shown in Fig. 8a. Under an applied field, the structure forms an accumulation layer at the dielectric-conducting oxide interface. This increased carrier concentration in the ITO lowers the permittivity due to the Drude model. Furthermore, ellipsometry was performed on the entire heterostructure, until self-consistency was achieved between the complex indices in the heterostructure and the respective permittivity for each individual material. The measurements indicated a large change in the refractive index between 25–75%, at the visible wavelengths in a 5 nm layer (Fig. 8b). For 2.5 V, at 500 nm wavelength the index change is Δn_{index} = 0.41 and at a wavelength of 800 nm the index change is Δn_{index} = 1.39 [60]. However, the work left some open and unanswered questions such as why were the Kramers–Kronig relations violated, and the physical picture of increasing optical loss with increasing carrier density (see above). Although this work did not fabricate an actual EOM, their pioneer work pointed out that modulation of the local refractive index within these structures, com-

bined with the high mode confinement achievable in plasmonic waveguides, could produce large changes in the effective index of propagating plasmonic modes, which gave ways to the future SPP EOM study as we will discuss next.

ITO has been implemented in a metal–insulator–metal (MIM) waveguide structure to demonstrate a subwavelength plasmonic modulator (Fig. 9a), for which a five percent change in the average carrier density (from 9.25×10^{20} to 9.7×10^{20} cm^{-3}) is observed [61]. The structure supports loosely bound SPP at a telecommunication wavelength of 1.55 μm owing to a MIM waveguide mode. A similar structure (Fig. 9b) based on a silicon-waveguide-integrated multilayer stack was fabricated and characterized. The logarithmic extinction ratio regarding to power up to 0.02 dB was achieved, which is much smaller than their prediction that 1 dB extinction ratio on 0.5 μm length. Moreover, there is always a trade-off between modulation depth and transmittance due to the high confinement achievable in the MIM waveguide and the high losses associated with both metal and ITO layers. However, the group showed the first AC modulation of ITO EOMs into the MHz range.

In 2012, a record-high extinction ratio of 1 dB/μm was demonstrated for a plasmonic modulator utilizing a metal-oxide-ITO stack on top of a silicon photonic waveguide (Fig. 10) [20]. Under an applied bias, the carrier concentration is changed from 1×10^{19} cm^{-3} to 6.8×10^{20} cm^{-3}, and the propagation length is varied from 1.3 to 43 μm. Also, the total insertion loss comprising of both the SOI-to-MOS coupling (–0.25 dB/coupler) and plasmonic MOS mode propagation (–0.14 dB/μm) were fairly low, which could achieve a total insertion loss as low as only about –1 dB for a 5 μm long modulator due to the good impedance match between the SOI and MOS mode and low ohmic losses from the plasmonic MOS mode [20, 67–69].

Recently, another characteristic of the SPP EOM deploying ITO as an active material was demonstrated by the Leuthold's team (2014); the hysteresis of the gate current and the optical transmission displays characteristics of a resistive random access memory (RRAM) (Fig. 10a) [70]. Note, the design is similar to that of Sorger's work (2012), and hence the observed ER of 1.2 dB/μm is expected [20]. However, by gradually altering the voltage an IV hysteresis is observed which indicates the memory effect of the switch, and the authors' claim arises from the metal pillars forming from the top metal through the gate oxide. The device demonstrates repeatability as indicated by a series of 50 consecutive measurements (Fig. 10b). Although the physical nature of the resistive switching mechanism is not fully understood, this work shows a new direction to utilize ITO as an active material.

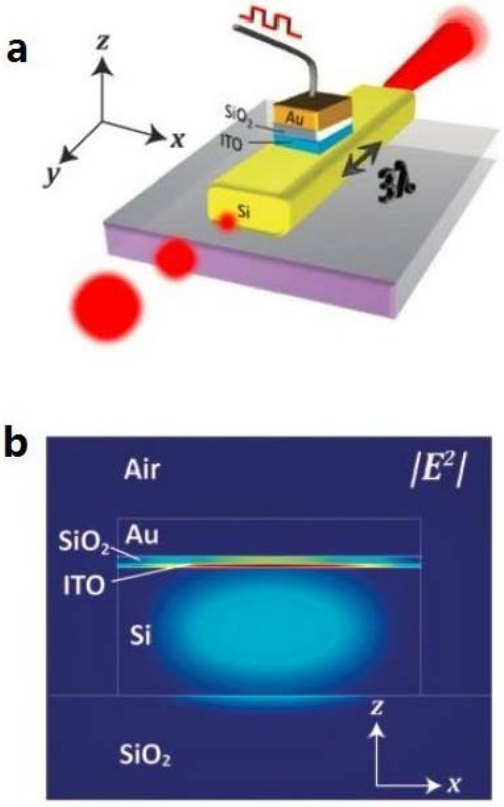

Figure 10: (a) Schematic of the waveguide-integrated, silicon-based nanophotonic modulator [20]. (b) Electric field density across the active fundamental MOS region of the modulator. The MOS design (with a gate oxide of about 30 nm) features a plasmonic optical mode, which concentrates the mode's electric field and allows for a good overlap with the active ITO layer.

6 Outlook and Conclusion

In addition to the experimental demonstrations briefly discussed above, there are a variety of theoretical proposals for TCO and/or ITO-based EOMs [37–39, 67]. Common to most of them is the usage of plasmonics to enhance the LMIs, resulting in small footprint and high-performance electro-optic properties.

In the context of PICs, TCO-based λ-size EOMs might be a logical next technological platform for hybrid networks on-chip. However, a variety of open questions are still outstanding in the field; (1) foremost, the debate of the nature of the index modulation of ITO is unsettled, and consists of two different viewpoints; one favours the carrier-based dispersion shift of ITO described by the Drude mode, whereas the second allocates the formation of metallic pillars that growth from the metal (typically Gold) contact through the electrical gate oxide [70]. Interestingly, the latter was reported in the supplementary in-

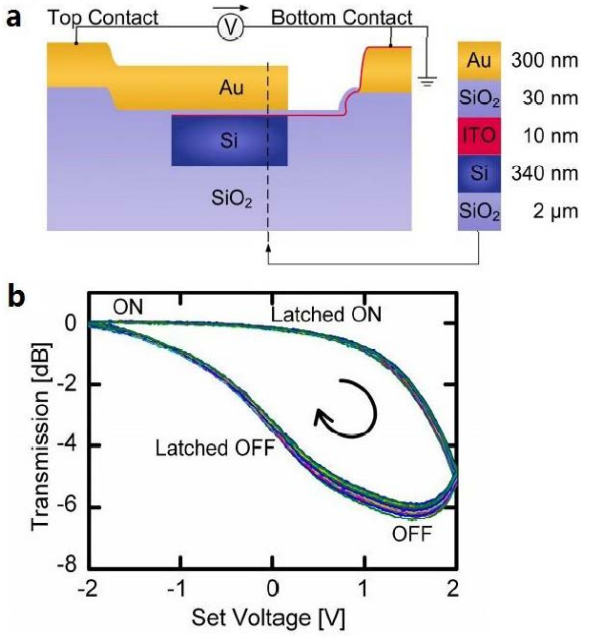

Figure 11: (a) Cross section view of the plasmonic memristor [70]. The device comprises a typical memristor MIM layers that further serve as a plasmonic waveguide on top of a silicon plasmonic waveguide. (b) Latching optical switch behavior for a 5 μm long device: 50 measurement cycles of the normalized optical transmission as a function of the set voltage showing a hysteresis and an extinction ratio of 6 dB.

formation of the Feigenbaum's original work already. In this regard, a detailed study correlating the device performance, with modelling and cross-sectional SEM images would be needed to solve this outstanding question on the modulation mechanism. (2) Based on our own ellipsometry work, we must conclude that this technique is very sensitive to the model type chosen and the fitting procedure. Thus, in order to make results comparable, detailed procedures to minimize the fitting errors should be followed. (3) The localized and selective doping ITO in a post-deposition process step to lower the contact resistance should be studied in more detail for future work.

In conclusion, TCOs, and particularly ITO, have been found to be intriguing candidates for strong refractive index modulation. The physical effect seems to point towards a strong carrier modulation of the TCO when biased near the ENZ point of ITO's permittivity. Early studies have demonstrated electro-optic modulation devices that utilize plasmonic field confinement and these TCOs. While this research field is still ongoing, those early demonstrations have shown the potential to deliver λ-size, ultra-low capacitance devices for future photonic integrated circuitry.

Acknowledgement: We acknowledge support from the Air Force Office of Scientific Research (AFOSR) under the award number FA9559-14-1-0215 and FA9559-14-1-0378.

References

[1] Baliga J., Ayre R., Hinton K., Sorin W.V., Tucker R.S., Energy consumption in optical IP networks, J. Lightw. Technol. 2009, 27, 2391–2403.
[2] Miller D.A.B., Device requirements for optical interconnects to silicon chips, Proc. IEEE. 2009, 97, 1166–1185.
[3] Miller D.A.B., Nanophotonic Devices: Beyond Classical Limits, Proc. OSA Incubator Meeting, Washington, DC. 14–16 May 2014.
[4] Rattner J., PLENARY: The Future of Silicon Photonics. Photonics in Switching. OSA, 2010.
[5] Udipi A.N., Muralimanohar N., Balasubramonian R., Davis A., Jouppi N.P., Combining memory and a controller with photonics through 3D-stacking to enable scalable and energy-efficient systems, Acm. Comp. Ar. 2011, 39.
[6] Interconnects. The International Technology Roadmap for Semiconductors. 2005. (Accessed September 10, 2014, at http://www.itrs.net/Links/2005ITRS/Interconnect2005.pdf.)
[7] Sun C., Chen C., Kurian G. *et al.*, DSENT-a tool connecting emerging photonics with electronics for opto-electronic networks-on-chip modeling. Networks on Chip (NoCS), 2012 Sixth IEEE/ACM Int. Symp. IEEE, 2012.
[8] Wassel H.M.G., Dai D., Tiwari M. *et al.*, Opportunities and challenges of using plasmonic components in nanophotonic architectures, IEEE Trans. Emerg. Sel. Topics Circuits Syst. 2012, 2, 154–168.
[9] Chen L., Shakya J., Lipson M., Subwavelength confinement in an integrated metal slot waveguide on silicon, Opt. Lett. 2006, 31, 2133–2135.
[10] Koos C., Vorreau P., Vallaitis T. *et al.*, All-optical high-speed signal processing with silicon–organic hybrid slot waveguides, Nat. Photonics. 2009, 3, 216–219.
[11] Gramotnev D.K., Bozhevolnyi S.I., Plasmonics beyond the diffraction limit, Nat. Photonics. 2010, 4, 83–91.
[12] Kirchain R., Kimerling L., A roadmap for nanophotonics, Nat. Photonics. 2007, 1, 303–305.
[13] Dionne J.A., Lezec H.J., Atwater H.A., Highly confined photon transport in subwavelength metallic slot waveguides, Nano Lett. 2006, 6, 1928–1932.
[14] Verhagen E., Spasenović M., Polman A., Kuipers L.K., Nanowire plasmon excitation by adiabatic mode transformation, Phys. Rev. Lett. 2009, 102, 203904.
[15] Bozhevolnyi S.I., Volkov V.S., Devaux E., Laluet J., Ebbesen T.W., Channel plasmon subwavelength waveguide components including interferometers and ring resonators, Nat. 2006, 440, 508–511.
[16] Jung K.Y., Teixeira F.L., Reano R.M., Surface plasmon coplanar waveguides: Mode characteristics and mode conversion losses, IEEE Photon. Technol. Lett. 2009, 21, 630–632.
[17] Steinberger B., Hohenau A., Ditlbacher H. *et al.*, Dielectric stripes on gold as surface plasmon waveguides, Appl. Phys. Lett. 2006, 88, 094104-094104.

[18] Krasavin A.V., Zayats A.V., Silicon-based plasmonic waveguides, Opt. Express. 2010, 18, 11791–11799.
[19] Nanophotonic Devices: Beyond Classical Limits, Proc. OSA Incubator Meeting, Washington, DC. 14–16 May 2014.
[20] Sorger V.J., Lanzillotti-Kimura N.D., Ma R.M., Zhang X., Ultra-compact silicon nanophotonic modulator with broadband response, Nanophotonics 2012, 1, 17–22.
[21] Ellmer K., Past achievements and future challenges in the development of optically transparent electrodes, Nat. Photonics. 2012, 6, 809–817.
[22] Mcmaster H.A., Conductive coating for glass and method of application, U.S. Patent No. 2, 429, 420, 1947.
[23] Vanboort H.J., Groth R., Low-pressure sodium lamps with indium oxide filters, Phil. Tech. Rev. 1968, 29, 47–48.
[24] Köstlin H.R.J., Lems W., Optical and electrical properties of doped In2O3 films, Phys. Status Solidi A. 1975, 29, 87–93.
[25] White D.L., Feldman M., Liquid-crystal light valves, Electron. Lett. 1970, 6, 837–839.
[26] Lampert C.M., Heat mirror coatings for energy conserving windows, Sol. Energy Mater. 1981, 6, 1–41.
[27] Hamberg I., Granqvist C.G., Evaporated Sn-doped In2O3 films: basic optical properties and applications to energy-efficient windows, J. Appl. Phys. 1986, 60, R123–R160.
[28] Betz U., Olsson M.K., Marthy J., Escolá M.F., Atamny F., Thin films engineering of indium tin oxide: Large area flat panel displays application, Surface and Coatings Technology 2006, 200, 5751–5759.
[29] Katayama M., Tft-lcd technology, Thin Solid Films 1991, 341, 140–147.
[30] Xiao X., Xu H., Li X., Li Z., Chu T., Yu Y., Yu J., High-speed, low-loss silicon Mach–Zehnder modulators with doping optimization, Opt. Express 2013, 21, 4116–4125.
[31] Lipson M., Compact electro-optic modulators on a silicon chip, IEEE J. Sel. Topics Quantum Electron., 2006, 12, 1520.
[32] Briggs R.M., Pryce I.M., Atwater H.A., Compact silicon photonic waveguide modulator based on the vanadium dioxide metal-insulator phase transition, Opt. Express 2010, 18, 11192–11201.
[33] Cui Y., Liu K., MacFarlane D.L., Lee J.B., Thermo-optically tunable silicon photonic crystal light modulator, Opt. Lett. 2010, 35, 3613–3615.
[34] Hassan K., Weeber J.C., Markey L. *et al.*, Thermo-optic plasmophotonic mode interference switches based on dielectric loaded waveguides, Appl. Phys. Lett. 2011, 99, 241110.
[35] Kalavrouziotis D., Papaioannou S., Giannoulis G. *et al.* 0.48 Tb/s (12 × 40 Gb/s) WDM transmission and high-quality thermo-optic switching in dielectric loaded plasmonics, Opt. Express 2012, 20, 7655–7662.
[36] Babicheva V., Lavrinenko A., Boltasseva A., Ultra-compact plasmonic waveguide modulators Kgs, Lyngby: Technical University of Denmark, 2013.
[37] Vasudev A.P., Kang J.H., Park J., Liu X., Brongersma M.L., Electro-optical modulation of a silicon waveguide with an "epsilon-near-zero" material, Opt. Express 2013, 21, 26387–26397.
[38] Lu Z., Zhao W., Shi K., Ultracompact electroabsorption modulators based on tunable epsilon-near-zero-slot waveguides, Photonics J. IEEE. 2012, 4, 735–740.
[39] Ye C., Sikander K., Li Z.R., Simsek E., Sorger V., lambda-Size ITO and Graphene-based Electro-optic Modulators on SOI, IEEE J. Sel. Topics Quantum Electron. 2014, 20, 4.
[40] Marezio M., Refinement of the crystal structure of In_2O_3 at two wavelengths, Acta Crystallographica 1966, 20, 723–728.
[41] Giusti G., Deposition and characterisation of functional ITO thin films, Diss. University of Birmingham, 2011.
[42] Nadaud N., Lequeux N., Nanot M., Jove J., Roisnel T., Structural Studies of Tin-D3ped Indium Oxide (ITO) and $In_4Sn_3O_{12}$, J. Solid State Chem. 1998, 135, 140–148.
[43] Jarzebski Z.M., Preparation and physical properties of transparent conducting oxide films, Phys. Status Solidi A. 1982, 71, 13–41.
[44] Rauf I.A., Yuan J., Effects of microstructure on the optical properties of tin-doped indium oxide thin films studied by electron energy loss spectroscopy, Mater. Lett. 1955, 25, 217–222.
[45] Fan J.C.C., Goodenough J.B., X-ray photoemission spectroscopy studies of Sn-doped indium-oxide films, J. Appl. Phys. 1977, 48, 3524–3531.
[46] Mott N.F., Friedman L., Metal-insulator transitions in VO_2, Ti_2O_3 and $Ti_{2-x}V_xO_3$, Philos. Mag. 1974, 30, 389–402.
[47] Slocombe D., Porch A., Pepper M., Edwards P.P., The Mott transition and optimal performance of transparent conducting oxides in thin-film solar cells, Energy Env. Sci. 2012, 5, 5387–5391.
[48] Materion, Inc. Transparent conductive oxide thin films. (Accessed September 10, 2014, at http://materion.com/~/media/Files/PDFs/Advanced{%}20Materials{%}20Group/ME/TechnicalPapers/Transparent{%}20Conductive_All.pdf.)
[49] Solieman A., Aegerter M.A., Modeling of optical and electrical properties of In_2O_3: Sn coatings made by various techniques, Thin Solid Films 2006, 502, 205–211.
[50] Kim Y.J., Jin S.B., Kim S.I., Choi Y.S., Choi I.S., Han J.G., Study on the electrical properties of ITO films deposited by facing target sputter deposition, J. Phys. D: Appl. Phys. 2009, 42, 075412.
[51] Chityuttakan C., Influence of deposition parameters on the quality of ITO films for photovoltaic application.
[52] Bender M., Seelig W., Daube C., Frankenberger H., Ocker B., Stollenwerk J., Dependence of oxygen flow on optical and electrical properties of DC-magnetron sputtered ITO films, Thin Solid Films 1998, 326, 72–77.
[53] Kurdesau F., Khripunov G., Da Cunha A.F., Kaelin M., Tiwari A.N., Comparative study of ITO layers deposited by DC and RF magnetron sputtering at room temperature, J. Non-Cryst. Solids 2006, 352, 1466–1470.
[54] Park J.O., Lee J.H., Kim J.J., Cho S.H., Cho Y.K., Crystallization of indium tin oxide thin films prepared by RF-magnetron sputtering without external heating, Thin Solid Films 2005, 474, 127–132.
[55] Guillen C., Herrero J., Comparison study of ITO thin films deposited by sputtering at room temperature onto polymer and glass substrates, Thin Solid Films 2005, 480, 129–132.
[56] Quaas M., Steffen H., Hippler R., Wulff H., Investigation of diffusion and crystallization processes in thin ITO films by temperature and time resolved grazing incidence X-ray diffractometry, Surf. Sci. 2003, 540, 337–342.
[57] Teixeira V., Cui H.N., Meng L.J., Fortunato E., Martins R., Amorphous ITO thin films prepared by DC sputtering for electrochromic applications, Thin Solid Films 2002, 420, 70–75.
[58] Tahar R.B.H., Ban T., Ohya Y., Takahashi Y., Tin doped indium oxide thin films: Electrical properties, J. Appl. Phys. 1998, 83, 2631–2645.
[59] Hamberg I., Hjortsberg A., Granqvist C.G., High quality transparent heat reflectors of reactively evaporated indium tin oxide, Appl. Phys. Lett. 1982, 40, 362–364.

[60] Feigenbaum E., Diest K., Atwater H.A., Unity-order index change in transparent conducting oxides at visible frequencies, Nano Lett. 2010, 10, 2111–2116.
[61] Melikyan A., Lindenmann N., Walheim S. *et al.*, Surface plasmon polariton absorption modulator, Opt. Express 2011, 19, 8855–8869.
[62] Brongersma M.L., Shalaev V.M., Applied physics the case for plasmonics, Sci. 2010, 328, 440–441.
[63] Moore G.E., Cramming more components onto integrated circuits (1965).
[64] Xu Q., Manipatruni S., Schmidt B., Shakya J., Lipson M., 12.5 Gbit/s carrier-injection-based silicon micro-ring silicon modulators, Opt. Express2007, 15, 430–436.
[65] Sorger V.J., Zhang X., Spotlight on plasmon lasers, Sci. 2011, 333, 709–710.
[66] Synowicki R.A., Spectroscopic ellipsometry characterization of indium tin oxide film microstructure and optical constants, Thin Solid Films 1998, 313, 394–397.
[67] Oulton R.F., Sorger V.J., Genov D.A., Pile D.F.P., Zhang X., A hybrid plasmonic waveguide for subwavelength confinement and long-range propagation, Nat. Photonics 2008, 2, 496–500.
[68] Sorger V.J., Ye Z., Oulton R.F., Experimental demonstration of low-loss optical waveguiding at deep sub-wavelength scales, Nat. Commun. 2011, 2, 331.
[69] Sorger V.J., Pholchai P., Cubukcu E., Strongly enhanced molecular fluorescence inside a nanoscale waveguide gap, Nano Lett. 2011, 11, 4907–4911.
[70] Hoessbacher C., Fedoryshyn Y., Emboras A., The plasmonic memristor: a latching optical switch, Optica 2014, 1, 198–202.